A Carbonic Anhydrase IX/SLC1A5 Axis Regulates Glutamine Metabolism Dependent Ferroptosis in Hypoxic Tumor Cells

Geetha Venkateswaran[1], Paul C. McDonald[1], Shawn C. Chafe[2], Wells S. Brown[1], Zachary J. Gerbec[1], Shannon J. Awrey[1], Seth J. Parker[3,4], and Shoukat Dedhar[1,4]

ABSTRACT

The ability of tumor cells to alter their metabolism to support survival and growth presents a challenge to effectively treat cancers. Carbonic anhydrase IX (CAIX) is a hypoxia-induced, metabolic enzyme that plays a crucial role in pH regulation in tumor cells. Recently, through a synthetic lethal screen, we identified CAIX to play an important role in redox homeostasis. In this study, we show that CAIX interacts with the glutamine (Gln) transporter, solute carrier family 1 member 5 (SLC1A5), and coordinately functions to maintain redox homeostasis through the glutathione/glutathione peroxidase 4 (GSH/GPX4) axis. Inhibition of CAIX increases Gln uptake by SLC1A5 and concomitantly increases GSH levels. The combined inhibition of CAIX activity and Gln metabolism or the GSH/GPX4 axis results in an increase in lipid peroxidation and induces ferroptosis, both *in vitro* and *in vivo*. Thus, this study demonstrates cotargeting of CAIX and Gln metabolism as a potential strategy to induce ferroptosis in tumor cells.

Introduction

Tumor hypoxia is one of the crucial factors that promotes cancer progression in solid tumors (1) and acts a major barrier to standard therapy (2, 3). The resilience of hypoxic cancer cells is attributed to the metabolic alterations that facilitate their adaptation to limited oxygen levels, thereby promoting survival (4, 5). Hence, understanding these metabolic adaptations is critical for developing strategies to effectively target hypoxic solid tumors. A major metabolic alteration in hypoxic cancer cells is to preferentially use glucose through glycolysis instead of oxidative phosphorylation for ATP production (6). A consequence of this shift is the buildup of acidic metabolic by-products in cells, resulting in an unfavorable, acidic intracellular pH (pHi). However, hypoxic cancer cells deploy pH regulatory enzymes and transporters to establish an optimal pH gradient that is conducive for survival (7, 8).

Carbonic anhydrases (CA) are metalloenzymes that play an important role in pH regulation by mediating the reversible hydration of carbon dioxide (CO_2) to bicarbonate and protons. Among the fifteen isozymes in this family, carbonic anhydrase IX (CAIX) and carbonic anhydrase XII (CAXII) are associated with cancer (9). CAIX/XII are hypoxia-induced, and their expression is often correlated with poor prognosis (10–14) and response to therapy (15–18) in various solid tumors. Furthermore, several studies have elucidated the roles of CAIX and CAXII in tumor growth (19–21) and metastasis (22–25) in various cancers. In addition, CAIX and CAXII are not widely expressed by normal tissues (26). These features make CAIX/XII ideal candidates for targeting solid tumors. The pharmacologic inhibition of CAIX/XII using the small molecule inhibitor, SLC-0111, has been shown to be effective in impeding tumor progression in preclinical studies (19, 20, 27, 28) and has advanced to a Phase-I clinical trial (29). Although SLC-0111 has shown promising effects in preclinical models, especially in combination with chemotherapy agents and immune check point blockade (19, 28, 30, 31), tumor recurrence is observed, demonstrating that hypoxic cancer cells adapt to inhibition of CAIX/XII activity. Therefore, studying the mechanism of adaptation to inhibition of CAIX/XII activity in hypoxic cancer cells will help in identifying novel combinatorial approaches to effectively treat solid tumors.

An unbiased proteomic screen to identify proteins that interact with CAIX in hypoxic cancer cells had previously identified the glutamine (Gln) transporter, solute carrier family 1 member 5 (SLC1A5), as a potential interactor (22), suggesting a potential role for CAIX in regulating Gln metabolism. Here, by using cell biological and biochemical approaches, we now demonstrate that CAIX associates and co-localizes with SLC1A5. The genetic or pharmacologic inhibition of CAIX increases Gln uptake and mediates an antioxidant response through the glutathione/glutathione peroxidase 4 (GSH/GPX4) axis to prevent ferroptosis. Combining CAIX inhibition with blockade of the central nodes within the Gln metabolism pathway leading to GSH production results in a significant increase in ferroptotic cell death of hypoxic cancer cells.

Materials and Methods

Cell lines and cell culture

The SUM159PT (RRID: CVCL_5423), Hs578t (RRID: CVCL_0332), and A549 (RRID: CVCL_0023) cell lines were a gift from S. Gorski, S. Aparicio, and A. Minchinton respectively (BC Cancer Research Institute). The MDA-MB-231 cell line (ATCC, catalog no. HTB-26,

[1]Department of Integrative Oncology, BC Cancer Research Institute, Vancouver, British Columbia, Canada. [2]Centre for Discovery in Cancer Research, McMaster University, Hamilton, Ontario, Canada. [3]British Columbia Children's Hospital Research Institute, Vancouver, British Columbia, Canada. [4]Department of Biochemistry and Molecular Biology, University of British Columbia, Vancouver, British Columbia, Canada.

Current address for W.S. Brown: AdMare BioInnovations, Vancouver, British Columbia, Canada.

Corresponding Author: Shoukat Dedhar, Department of Integrative Oncology, BC Cancer Research Institute, 675 West 10th Ave, Vancouver, British Columbia V5Z 1L3, Canada. E-mail: sdedhar@bccrc.ca

Mol Cancer Ther 2023;22:1228–42

doi: 10.1158/1535-7163.MCT-23-0041

RRID: CVCL_0062) was obtained from ATCC and the 4T1Luc+ cells have been previously described (32). The SUM159PT cells were maintained in DMEM with 10% FBS, 1× nonessential amino acids, 5 μg/mL insulin, and 1 μg/mL hydrocortisone. The Hs578t cells were maintained in DMEM with 10% FBS and 10 μg/mL insulin. The MDA-MB-231 and A549 cell lines were maintained in DMEM with 10% FBS. The SUM159PT $CA9^{KO}$ and MDA-MB-231 CAIXBirA* cell lines were grown as previously described (22, 33). All cell lines were authenticated using short tandem repeat DNA profiling by a commercial testing facility (Genetica, Burlington, NC) and screened for mycoplasma using the LookOut Mycoplasma test (Sigma, catalog no. MP0035) or DNA staining test. The latest *Mycoplasma* testing for 4T1Luc and SUM159 using LookOut Mycoplasma kit was performed in June 2019 and November 2021, respectively. DNA staining test was performed routinely for all the cell lines used in study. The latest DNA staining test on all cell lines was performed in November 2021. For experiments that required Gln-free or altered Gln levels, the cells were cultured in Gln-free media DMEM supplemented with the same supplements as described above for respective cell lines. To alter the Gln level in media, L-Gln was added to the Gln-free media to required final concentrations. Cells were maintained at 21% oxygen (O_2) and 5% CO_2 by routinely passaging every 2 to 3 days. For the hypoxia experiments, the cells were grown at 1% O_2, 94% nitrogen (N_2), and 5% CO_2. All cell lines were used for experiments within 20 passages.

Chemicals

NuPAGE MOPS SDS running buffer (Invitrogen, NP0001); cOmplete Protease Inhibitor Cocktail (Millipore, 11697498001); SuperSignalWest Femto (ThermoFisher, #34095); UltraLink Resin (ThermoFisher, 53132); Pierce 16% Formaldehyde (w/v) (ThermoFisher, 28908); Prolong Diamond Antifade mountant (ThermoFisher, P36970); L-[3,4–3H(N)]-Glutamine (Perkin Elmer, NET551250UC); Pico-Fluor-15 (Perkin Elmer); L-Buthionine-(S,R)-sulfoxamine (Sigma, B2515); V-9302 (Selleckchem, S8818); CB839 (Selleckchem, S7655); RSL3 (Selleckchem, S8155); Ferrostatin-1 (Cayman Chemical, 17729); Nec-1s (Biovision, 2263); Z-VAD-FMK (Selleckchem, S7023); Deferoxamine mesylate (Sigma, D9533); Trolox (Sigma, 238813); SLC-0111, Compound 11 and Compound 13 have been previously described (27); BODIPY 581/591 undecanoic acid (ThermoFisher, D3861); CM-H2DCFDA (ThermoFisher, C6827); Sytox Green nucleic acid stain (ThermoFisher, S7020); HCS NuclearMask red stain (ThermoFisher, H10326); with ImmPRESS HRP Universal Antibody (Vector Laboratories, MP-7500); DAB Substrate Kit, Peroxidase HRP (Vector Laboratories, SK-4100); TransIT-LT1 transfection reagent (Mirus Bio, 2304); Doxycycline (Dox; Sigma-Aldrich, D9891).

Chemical structure and synthesis of SLC-0111

The structure and full method of synthesis for the ureido-substituted benzenesulfonamide, SLC-0111 (refs. 28, 29) [also known as Compound 7 (ref. 27) and U-104 (ref. 20)], has been published previously (27).

Antibodies

Western blotting

Mouse anti-human CAIX (R and D Systems, MAB2188, RRID: AB_2066530); mouse IgG2A (R and D Systems, MAB003, RRID: AB_357345); goat anti-human CAIX (R and D Systems, AF2188, RRID:AB_416562) – 1:1,000; rabbit anti-human ASCT2 (Cell Signaling Technology, 8057, RRID:AB_10891440) – 1:500; mouse anti-vinculin (Millipore, MAB3574, RRID:AB_2304338) – 1:1,000; rabbit anti-human glutaminase-1 (GLS1; Abcam, ab156876, RRID:AB_2721038) – 1:500; mouse anti-human GCLC (Santa Cruz Biotechnology, sc-390811, RRID: AB_2736837) – 1:500; mouse anti ß-actin (Sigma-Aldrich, A5441, RRID: AB_476744).

Immunofluorescence and proximity ligation assay staining

Goat anti-human CAIX (AF2188) and rabbit anti-human ASCT2 (8057) were used at a dilution of 1:100. Alexa Fluor 488 AffiniPure donkey anti-rabbit (Jackson ImmunoResearch Labs, 711–545–152, RRID:AB_2313584); Alexa Fluor 555 donkey anti-goat (Thermo Fisher Scientific, A-21432, RRID:AB_2535853).

IHC staining

Mouse anti human CAIX M75 (Bioscience, AB1001) – 1:200; mouse anti-human GCLC (Santa Cruz, sc390811) – 1:50; rabbit anti-human CD71 (Cell Signaling Technology, 13208, RRID:AB_2798150) – 1:50; rabbit anti–4-hydroxynonenal (4-HNE; Abcam, ab46545, RRID: AB_722490) – 1:100.

Western blotting

Samples were lysed in RIPA buffer [50 mmol/L Tris-HCl, pH 7.6, 150 mmol/L NaCl, 0.1% (w/v) SDS] containing 1 mmol/L Na_3VO_4, 2 mmol/L NaF and cOmplete protease inhibitor. About 5 to 10 μg of protein was analyzed by 4% to 12% Bis-Tris gradient gel in 1× NuPAGE MOPS SDS running buffer. Gels were transferred to PVDF membranes for 1 hour at 100 V in ice-cold Tris-Glycine transfer buffer containing 20% methanol. The PVDF membranes were methanol-fixed briefly and incubated with primary antibodies in 5% skim milk in TBST overnight at 4°C, followed by washes with TBST for 3×10 minutes and incubation with horseradish peroxidase (HRP)-conjugated secondary antibody in 5% skim milk in TBST for 1 hour at room temperature. After subsequent washes with TBST, detection was performed by incubation with Supersignal West Femto chemiluminescence reagents and visualization using a Chemidoc XRS+ imaging system (Bio-Rad Laboratories). ß-actin or vinculin were used as loading controls.

Co-immunoprecipitation

Cells were cultured at 1% or 21% O_2 for 72 hours. After 72 hours, cells were washed with 1X PBS and lysed with ice-cold NP-40 buffer (1% NP-40, with cOmplete protease inhibitor cocktail, 1 mmol/L Na_3VO_4, 2 mmol/L sodium fluoride, pH 7.4) using a cell scraper and centrifuged to remove cell debris. One milligram of protein was immunoprecipitated at 4°C overnight using either 20 μg of mouse anti-huCAIX antibody or IgG isotype control with Protein A/G Agarose. The resin was washed 4 times with NP-40 buffer pH 8.0, resuspended in sample buffer, and boiled at 100°C for 10 minutes. The supernatant was separated from the resin by centrifugation using a polypropylene spin column for 1 minutes, at 4,000 rpm. All samples were loaded on SDS–PAGE gels and Western blots were performed as described above.

Immunofluorescence staining

Cells were seeded on glass coverslips in a 24-well plate and cultured in 1% or 21% O_2 for 72 hours. For immunofluorescence (IF) staining, cells were quickly washed with HBSS and fixed with 4%paraformaldehyde for 15 minutes at room temperature. Followed by two washes in 1XPBS, cells were incubated with blocking buffer (HBSS + 10% FBS) for 30 minutes and then incubated with CAIX antibody for 30 minutes at room temperature. The primary antibody incubation was followed by two washes with 1XPBS and then cells were permeabilized with 0.1% Triton solution for 10 minutes.

Cells were then incubated with SLC1A5 antibody at 4°C overnight. Post incubation, the cells were washed twice and then incubated with fluorescence-labeled secondary antibodies (antiRb-488 and antiGt-555) for an hour at room temperature, washed subsequently, and counterstained with Hoescht for 5 minutes. The coverslips were mounted on a glass slide using the Prolong Diamond Antifade mountant. Cells were imaged at 60× oil objective in the Nikon A1-si Confocal & TIRF microscope.

Proximity ligation assay

Cells were prepared for the experiment using the same protocol carried out for IF staining. Proximity ligation assay (PLA) was performed using the Duolink In Situ kit (DUO92101, Sigma) following the instructions provided by the manufacturer with the following modifications. After the blocking step, primary antibody incubations were performed at the incubation time and temperature that was used for IF staining. The cells were counterstained with Hoescht 33342 and mounted using the Prolong Diamond Antifade mountant. Cells were imaged at 60x oil objective in the Nikon A1-si Confocal & TIRF microscope.

Gln uptake assay

Cells were cultured in 12-well plates for 72 hours at 1% O_2 in the presence of indicated treatments. For the uptake assay, cells were washed with HEPES-HBSS buffer and incubated with the buffer for 15 minutes. Following the incubation, the buffer was replaced with 500 μL of HEPES-HBSS buffer containing L-[3,4–3H(N)]-Glutamine at a final concentration of 1 μCi/mL. The cells were incubated with the tracer for 0, 1, 5, 10, and 15 minutes, washed with ice-cold HEPES-HBSS buffer and lysed using 500 μL of 0.1 N NaOH. 400 μL of the lysate were mixed with 5 mL of Pico-Fluor scintillation cocktail and counts per minute (CPM) were measured using the Beckman L6500 scintillation counter. 100 μL of the lysate was aliquoted for protein quantification for normalization. The normalized CPM from the untreated condition was set as 100% and the relative change with treatment was measured. All of the steps prior to cell lysis were carried out in a hypoxia chamber maintained at 1% O_2 and 5% CO_2. Each experimental condition had three technical replicates.

CAIX activity assay

In-Cell CAIX catalytic activity assays were carried out as described (33). Assays were performed using SUM159PT cells following a 72-hour incubation in 1% O_2. Cells were harvested using 0.5 mmol/L EDTA in PBS. For each sample, 5×10^5 cells were suspended in 100 μL of CO_2-free isotonic buffer [20 mmol/L HEPES, 130 mmol/L NaCl, and 5 mmol/L KCl (pH 8.0)] in a 2-mL flat bottom vial equipped with an 8-mm magnetic stir bar. SLC-0111 was added to the cell suspension to a final concentration of 50 μmol/L or an equivalent volume of DMSO vehicle was added, and the sample was incubated at room temperature for 30 minutes. An additional 700 μL of ice-cold buffer was then added to the cell-inhibitor mixture, and a narrow pH electrode (Accumet) was immersed in the sample and equilibrated for 3 minutes. A total of 200 μL of CO_2-saturated water was added to initiate the assay, and pH readings were recorded at 5-second intervals for up to 150 seconds. The change in pH was plotted as a function of time. To determine the rate of spontaneous CO_2 hydration, measurements were performed on cell-free ("buffer") samples. The increase in hydration rate above the spontaneous rate is a measure of CA activity. Three replicates were assayed for each condition evaluated in the assay.

GSH assay

Cells were prepared using the same protocol as the Gln uptake experiment. After 72 hours of treatment, GSH measurement was carried out by a luminescence-based assay using the kit GSH/GSSG-Glo (Promega, V6611) according to the manufacturer's instructions. The luminescence signal was measured by SpectraMax i3x plate reader (Molecular devices).

Cytotoxicity studies

Cells were seeded and cultured at 21% O_2 overnight. The following day, drug treatments were carried out by diluting drugs at required final concentrations in media containing the cell viability dye, SYTOX Green nucleic acid stain (1:20,000 dilution; 250 nmol/L final). Treated cells were grown at 1% O_2 for 72 hours and then stained with HCS NuclearMask Red stain to determine the total number of cells. The signal from the stains was evaluated using a Incucyte ZOOM (Essen Biosciences) imaging system. The cell viability was calculated as % cytotoxicity = [#dead cells (green)/#red cells (total number of cells)]*100.

Synergy analysis

The web-based application SynergyFinder 3.0 (https://synergyfinder.fimm.fi/) was used to analyze multidrug synergies (34). Data were uploaded as appropriately formatted tables and % inhibition was selected as a readout. Four-parameter logistic regression (LL4) curve fitting was applied and automated outlier detection was toggled "on". The zero interaction potency reference model was used for synergy scoring and the correction parameter was toggled "on". For Synergy scores greater than 10, drug interactions were considered to be synergistic. For synergy scores from 2 to 10 drug interactions were considered to be additive with scores from 9 to 10 approaching synergy.

Cellular and lipid reactive oxygen species measurements

Cells were prepared using the same protocol as cytotoxicity experiments. After the treatment incubation, cells were washed with HEPES-HBSS and stained with 0.5 μmol/L CM-H2DCFDA [cellular reactive oxygen species (ROS)] or 2 μmol/L BODIPY 581/591 C11 (Lipid ROS) for 15 minutes at 37°C in 1% O_2. Cells were then washed and trypsinized. Collected cells were washed with HBSS + 2% FBS, resuspended in the same buffer, and analyzed by FACS using a BD LSRII Fortessa. Data were analyzed in FlowJo (RRID:SCR_008520). Calculations for BODIPY-C11 were carried out according to the method followed in a recent study (35).

Spheroids

SUM159 cells were seeded at 1,000 cells/well of an ultralow attachment 96-well plate in the previously described complete media. After the cells clumped up and formed a spheroid of 100 to 200 μmol/L (about 72 hours), the indicated drug treatments were carried out in the presence of the cell viability dye, SYTOX Green nucleic acid stain, at a 1:20,000 dilution (250 nmol/L). The drugs were refreshed every 3 to 4 days. Cytotoxicity of spheroids was evaluated in real-time by measuring the green signal by live imaging using Incucyte ZOOM.

Animal studies

All studies were performed in accordance with University of British Columbia and BC Cancer Research Institute Animal Care Committee guidelines under approved animal ethics protocol A18–0132. A total of 1×10^6 SUM159PT shGCLC-5 cells were injected into the mammary fat pad of 10- to 14-week-old female NOD-scid IL2Rgamma null

(NSG) (RRID:BCBC_4142) mice in a solution consisting of 80% Matrigel/20% saline. Tumor growth was tracked by digital caliper measurements, and volumes were calculated using the modified ellipsoid formula ($l \times w^2 \times \pi/6$). Once the average tumor volume reached ~75 mm^3, mice were randomized to ensure equivalent average volumes and assigned into six treatment groups including, No Dox (1% Sucrose), Dox (2 mg/mL in 1% sucrose), Vehicle, SLC-0111 (100 mg/kg), Vehicle + Dox and SLC-0111 + Dox. Vehicle and SLC-0111 were dosed once daily by oral gavage and Dox was administered in drinking water. Saline was administered by subcutaneous injection once daily to prevent dehydration due to reduced fluid intake from treatments in drinking water. For survival analyses, a surrogate threshold was used, and survival events occurred once tumors reached approximately 400 mm^3. Tumors were harvested and fixed in formalin and embedded in paraffin for IHC.

IHC and IF staining on tumor sections

Five micron sections of formalin-fixed, paraffin-embedded tissue were deparaffinized, rehydrated and antigen retrieval was performed by microwaving in 10 mmol/L citrate buffer, pH 6.0 for 10 minutes. Sections were incubated with 3% H_2O_2 for 15 minutes to quench endogenous peroxidase activity, followed by blocking for an hour at room temperature in blocking buffer (3% skim milk, 1% BSA in PBS). Tissue sections were incubated with primary antibody diluted in blocking buffer at dilutions indicated above for overnight at 4°C. After 3 washes, the sections were incubated with ImmPRESS HRP antibody for 30 minutes at room temperature. The DAB staining was carried out using DAB peroxidase HRP Substrate according to the manufacturer's instructions. Tissues were counterstained with hematoxylin (Leica Biosystems). For quantification, at least 5 randomly selected fields of view at 10x magnification were imaged from 1 section/tumor with at least 4 tumors for each treatment group. The mean intensity of positive staining was quantified using ImageJ Fiji (RRID:SCR_003070).

Processing of tumor sections for IF staining was performed similar to the protocol for IHC staining and the IF staining of sections was performed using the same conditions used for used for IF staining of cells.

Generation of cell lines

HEK293 cells (RRID:CVCL_0045) were seeded at 50,000/cm^2. The following day, cells were transfected with 0.9 μg pSPAX; 0.1 μg of pVSVG; and 1 μg of the target plasmid using TansIT-LT1 transfection reagent. The media was replaced with fresh media the following day and continued to grow for 48 hours. After 48 hours, the virus was harvested by passing the media through a 0.45 μmol/L filter. The virus was added to SUM159PT WT or SUM159PT $CA9^{KO}$ cell lines along with polybrene and incubated overnight. Antibiotic selection with 3 μg/mL Puromycin for the knockdown cell lines or 1 mg/mL G418 for the CAIX mutant cell lines was initiated the following day and cells were continued to be cultured in the presence of selection antibiotics. The CAIX mutant cell lines FL; ΔIC and H200A were generated using plasmids that were developed previously (22). The Dox-inducible knockdown cell lines were generated using pTRIPZ inducible short hairpin RNA (shRNA) plasmids from Horizon discovery. The information of the gene targets used in the study is provided in Supplementary Table S1.

For experiments involving induction of shRNA using Dox, cells were seeded into 6-well plates cultured in the presence or absence of 1 μg/mL Dox and cultured at 21% O_2 for 72 hours. Followed by the Dox induction, cells were lysed for Western blots and seeded for cytotoxicity studies as described above.

LC/MS analysis for GSH/GSSG ratio

SUM159 cells were seeded at 10,000 cells/cm^2 in the presence or absence of 100 μmol/L SLC-0111. After 72 hours of treatment, cells were washed with ice-cold PBS and extracted with 80% ice cold methanol by scraping. The extracts were analyzed for GSH and GSSG by liquid chromatography–mass spectrometry (LC-MS) (36).

Data availability

The data generated in this study are available upon request from the corresponding author.

Results

CAIX associates with SLC1A5 nutrient transporter in cancer cells

The SLC1A5 Gln transporter was identified in a BioID proteomic screen carried out to identify potential CAIX proximity interactors (22). This was of interest because SLC1A5 expression, like CAIX, is induced in hypoxia (37) and it is also a critical regulator of Gln metabolism in cancer cells (38, 39). Thus, to determine and validate the potential functional association between CAIX and SLC1A5 in hypoxic cancer cells, we first used a clustered regularly interspaced short palindromic repeats (CRISPR)-Cas9 knockout (KO) approach to deplete *CA9* ($CA9^{KO}$) in MDA-MB-231 and SUM159PT triple-negative breast cancer (TNBC) cells and evaluated the levels of SLC1A5 expression in hypoxia. In both cell lines, we observed that the level of SLC1A5 increased in response to depletion of CAIX, compared with control cells (**Fig. 1A** and **B**), suggesting that CAIX and SLC1A5 might interact functionally in cancer cells in hypoxia.

Next, we carried out several approaches to validate the interaction. First we assessed the interaction using co-immunoprecipitation (co-IP) of these proteins from the exogenous CAIX expressing MDA-MB-231-CAIX-BirA* cell line previously used for the BioID studies (22). Given that the cells exogenously express CAIX, the cells were cultured in normoxia (21% O_2) for 72 hours and evaluated for interaction of CAIX and SLC1A5 in cell lysates. In line with the findings from the BioID study, CAIX associated with SLC1A5 (**Fig. 1C**). We then performed co-localization studies using IF staining for the proteins under the same conditions used for co-IP and observed that the two proteins co-localized at the cell membrane (**Fig. 1D**). The associations are particularly evident in migration fronts resembling lamellipodia and pseudopodia-like protrusions, indicating a potential role of the interaction in migrating cells.

Having investigated the interaction of CAIX with SLC1A5 in a cell line exogenously expressing CAIX, we further explored this interaction in additional cancer cell lines under endogenous conditions in hypoxia. Similar to the findings with MDA-MB-231-CAIX-BirA* cell line, co-IP analyses showed that CAIX interacts with SLC1A5 compared with the corresponding isotype control in two different cell lines: the SUM159PT TNBCs, and the A549 non–small cell lung cancer cells. (**Fig. 1E**). Furthermore, the proteins co-localized at the cell membrane in both cell lines (**Fig. 1F**) and also co-localized *in vivo* in a SUM159PT orthotopic model of breast cancer (Supplementary Fig. S1A). Moreover, we observed that, similar to our *in vitro* findings, tumor regions expressing lower levels of CAIX demonstrated increased levels of SLC1A5 (Supplementary Fig. S1A).

To further validate the association, we measured the interaction of CAIX and SLC1A5 using a PLA and observed a significant increase in the interaction signal compared with the negative controls (**Fig. 1G** and **H**), suggesting that the two plasma membrane proteins are localized within 10 to 20 nm of each other (40). Interestingly, this association did not change (Supplementary Fig. S1B and S1C) when

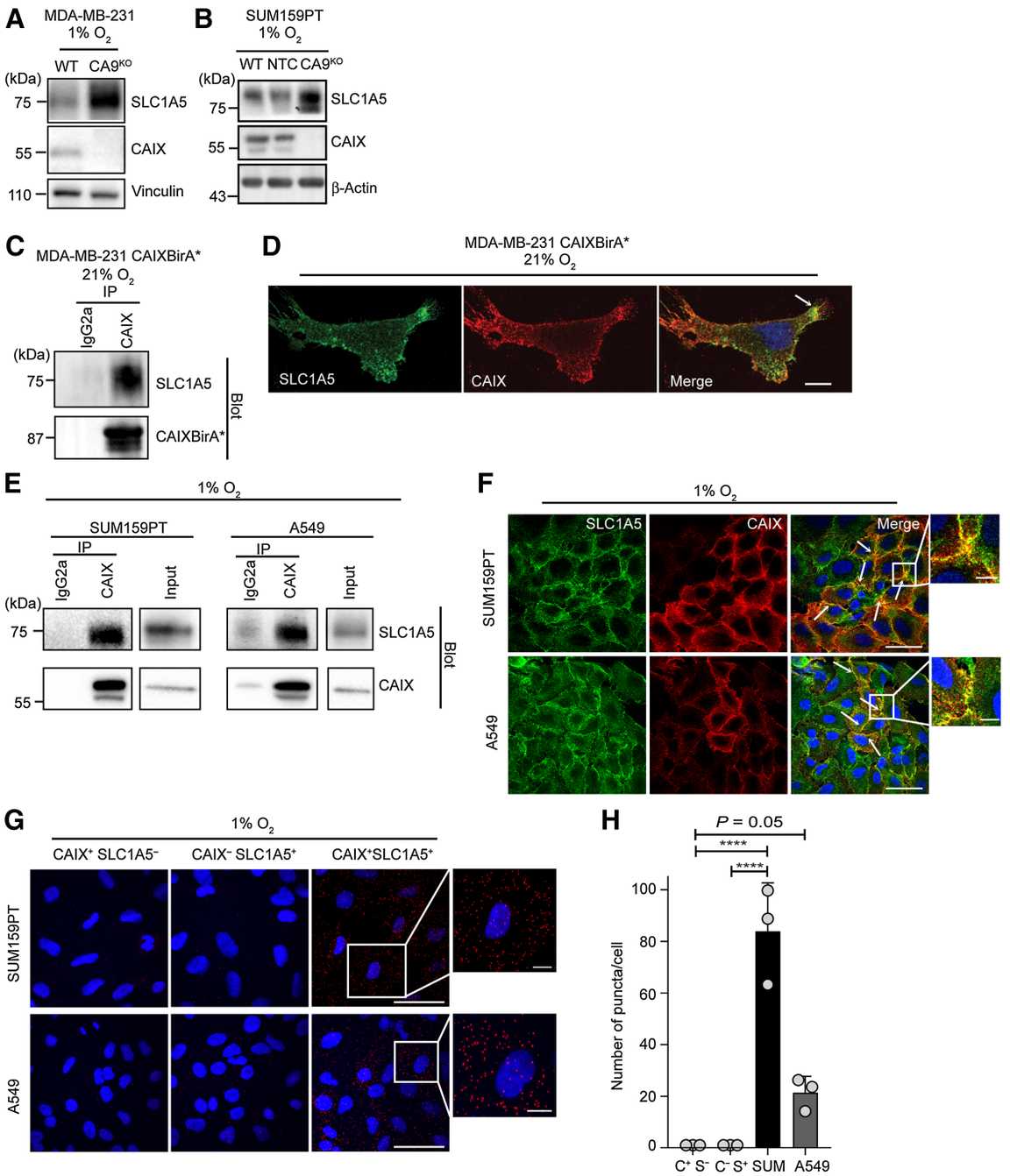

Figure 1.

CAIX associates with SLC1A5 in hypoxic cancer cells. **A,** Expression of SLC1A5 and CAIX shown by Western blotting of MDA-MB-231 WT and *CA9*^{KO} cell lysates. Cells were cultured at 1% O_2 for 72 hours. Blots are representative of two independent experiments. **B,** Expression of SLC1A5 and CAIX shown by Western blotting of SUM159 WT, NTC (non target control) and *CA9*^{KO} cell lysates. Cells were cultured at 1% O_2 for 72 hours. Blots are representative of two independent experiments. **C,** Interaction of SLC1A5 and CAIX shown by co-IP analyses in MDA-MB-231 CAIXBirA* cell lysates. Cells were cultured at 21% O_2 for 72 hours. IgG2a was used as an isotype-specific control for the IP. Blots are representative of two independent experiments. **D,** Co-localization (yellow; arrows) of SLC1A5 (green) and exogenously expressed CAIX (red) in MDA-MB-231 CAIXBirA* cells shown by IF staining. Cells were cultured at 21% O_2 for 72 hours. Scale bar, 10 μm. **E,** Interaction of SLC1A5 and endogenous CAIX shown by co-IP analyses in SUM159PT and A549 cell lysates. Cells were cultured at 1% O_2 for 72 hours. IgG2a was used as an isotype-specific control for the IP. Blots are representative of two independent experiments. **F,** Co-localization (yellow; arrows) of SLC1A5 (green) and endogenous CAIX (red) in SUM159PT and A549 cells shown by IF staining. Cells were cultured at 1% O_2 for 72 hours. Scale bars, 50 μm; 10 μm (zoomed image). **G,** Interaction of SLC1A5 and CAIX (Red puncta) in SUM159 and A549 cells shown by PLA. Cells were cultured at 1% O_2 for 72 hours. Treatments with only SLC1A5 antibody (CAIX$^-$ SLC1A5$^+$) and only CAIX antibody (CAIX$^+$SLC1A5$^-$) were used as negative controls for the assay. Scale bars, 50 μm; 10 μm (zoomed image). **H,** Quantification of the puncta from (**G**) for SUM159PT and A549 cells. Puncta were quantified from three images for each condition, having at least 20 cells in each image. See also Supplementary Fig. S1.

the activity of CAIX was inhibited with a specific inhibitor of CAIX, SLC-0111 (27–29).

Because CAIX is a transmembrane integral plasma membrane protein, we wanted to determine whether the intracellular domain of CAIX played a role in the association between SLC1A5 and CAIX. For this, we exogenously expressed either the full length CAIX (FL), an intracellular domain deletion mutant of CAIX (ΔIC) or a catalytically inactive mutant (H200A) in SUM159PT $CA9^{KO}$ cells and assessed the interaction between CAIX and SLC1A5 by PLA. The protein levels of CAIX were comparable between SUM159PT-FL, ΔIC, and H200A cells (Supplementary Fig. S1D). The H200A catalytically inactive CAIX mutant had higher levels of SLC1A5, which were comparable with CAIX KO (Supplementary Fig. S1D). Furthermore, the CAIX activity was similar to SLC-0111 treatment or $CA9^{KO}$, indicating the effective abrogation of catalytic activity in the H200A cell line (Supplementary Fig. S1E). Interestingly, while the interaction between CAIX and SLC1A5 remained relatively unchanged in the catalytically inactive H200A expressing cell line, aligning with our observations in response to SLC-0111 treatment, the interaction between CAIX and SLC1A5 was significantly reduced in the cells expressing the ΔIC variant of CAIX, relative to that in cells expressing the FL CAIX (Supplementary Fig. S1F and S1G). Together, these data suggest that CAIX and SLC1A5 associate within close proximity in hypoxic cancer cells, and that the association may involve the intracellular domain of CAIX.

Genetic depletion or inhibition of CAIX activity increases Gln uptake

To determine a potential role of CAIX activity in the function of SLC1A5, we carried out a series of experiments measuring Gln uptake in a variety of tumor cell types. In addition to SUM159PT and MDA-MB-231 TNBCs, and A549 lung cancer cells in which we have already demonstrated an association between the two proteins (**Fig. 1**; Supplementary Fig. S1), we also included two additional breast cancer cell lines, Hs578t and luciferase (Luc) positive 4T1Luc, to assess whether these proteins interacted functionally across a broad range of cancer cell types.

First, because SLC1A5 functions to transport Gln into cells, we classified these cell lines based on their dependency on Gln for survival and growth. The SUM159PT, A549 and 4T1Luc cell lines were all found to be highly dependent on Gln, with a significant decrease in proliferation observed in Gln-depleted media (**Fig. 2A**). In contrast, the Hs578t and MDA-MB-231 cell lines were not very sensitive to Gln deprivation, with less than 40% decrease in proliferation observed for these cells (**Fig. 2A**). Interestingly, we observed that Gln-dependent cells showed the highest levels of expression of CAIX in hypoxia (**Fig. 2B**), suggesting a potential role of the level of CAIX expression on Gln dependency. Using this panel of cell lines, we next investigated the effect of pharmacologic inhibition of CAIX activity with SLC-0111 on Gln uptake. We observed that in the Gln-dependent cell lines, inhibition of CAIX/XII activity resulted in increased Gln uptake (**Fig. 2C**; Supplementary Fig. S2A), whereas Gln uptake in the Gln-independent cell lines remained unchanged (**Fig. 2D**; Supplementary Fig. S2A). To ensure that the changes observed in Gln uptake with CAIX/XII inhibition were not limited to SLC-0111 treatment, we extended our findings with other small-molecule inhibitors in the ureidosulfonamide class, such as Compound 11 and Compound 13 (27). Treatment with these inhibitors also showed an increase in Gln uptake compared with the no treatment control (Supplementary Fig. S2B).

Next, to determine whether the effect of inhibiting the catalytic activity of CAIX could be phenocopied by genetic depletion of CAIX expression, we measured Gln uptake in $CA9^{KO}$ SUM159PT and MDA-MB-231 cell lines (**Fig. 2E** and **F**). Similar to the response observed with the treatment of SLC-0111, $CA9^{KO}$ resulted in increased Gln uptake in SUM159PT (Gln-dependent) but not in MDA-MB-231 (Gln-independent) cells (**Fig. 2F**). Furthermore, Gln uptake was significantly increased in the SUM159PT cells expressing either the ΔIC or H200A forms of CAIX (Supplementary Fig. S2C), similar to that observed after genetic depletion or pharmacologic inhibition of CAIX.

To determine whether the observed increase in Gln uptake upon inhibition or depletion of CAIX is mediated by SLC1A5, we suppressed the expression of SLC1A5 using Dox-inducible shRNA-mediated knock down in the SUM159PT cell line (**Fig. 2G**) and measured Gln uptake in the presence or absence of SLC-0111. Gln uptake in the SUM159-shNS (non-specific target control) showed an approximately 40% increase with SLC-0111 treatment compared with the untreated condition and is comparable with that observed in SUM159PT-WT cell line (**Fig. 2H**). However, Dox-inducible knockdown of SLC1A5 (shSLC1A5) decreased the Gln uptake by approximately 40% compared with the SUM159PT-shNS or the SUM159PT-shSLC1A5 cells without Dox treatment (**Fig. 2H**). Interestingly, the increase in Gln uptake observed with SLC-0111 treatment also decreased to same level as observed in the SLC1A5 knock down cells (**Fig. 2H**).

These data suggest that hypoxic cancer cells increase Gln uptake in a SLC1A5-dependent manner upon CAIX inhibition, indicating a potential compensatory mechanism to overcome the stress response of inhibiting CAIX function.

The combined loss of CAIX activity and Gln metabolism increases cytotoxicity of hypoxic cancer cells

The increased Gln uptake observed in hypoxic cancer cells upon depletion of CAIX expression/activity led us to investigate whether the combined inhibition of CAIX and Gln metabolism causes lethal effects in cells. To study this, we used the three cell lines, SUM159PT, 4T1Luc, and A549, which showed an increase in Gln uptake with CAIX depletion. We first tested the levels of cytotoxicity when SUM159PT–wild-type (WT) cells treated with SLC-0111 or the SUM159PT- $CA9^{KO}$ cells without any treatment were cultured under hypoxia in Gln-free, complete media. As shown in **Fig. 3A** and **B**, the susceptibility of $CA9^{KO}$ cells to cell death was increased in the absence of Gln. Similarly, the level of cytotoxicity exhibited by SUM159PT-WT cells was increased upon SLC-0111 mediated inhibition of CAIX in Gln-free media (**Fig. 3A** and **B**). Furthermore, the SUM159PT-WT cells showed a threshold response to treatment with increasing concentrations of SLC-0111, with Gln concentrations of 0.5 mmol/L and above preventing cell death (**Fig. 3C**).

Next, we investigated the effect of combining SLC-0111 with inhibitors that target different steps involved in the Gln transport and metabolism (**Fig. 3D**). First, we tested the combination of SLC-0111 with V-9302, a small molecule antagonist of SLC1A5 (refs. 41, 42; **Fig. 3E**) and observed a dose-dependent increase in cytotoxicity with the combination, compared with single treatments, in the SUM159PT-WT cells (**Fig. 3E**). Similarly, in the 4T1Luc cells, we observed a dose-dependent increase in cytotoxicity in response to the combination at higher doses of SLC-0111 (**Fig. 3F**).

The significant increase in cytotoxicity observed when SLC-0111 was used in combination with V-9302 suggested that this drug combination may exhibit synergy. Analysis of the multidrug combination response data using SynergyFinder 3.0, a web-based software tool for multidose combination data analytics (34), showed that the combination of SLC-0111 and V-9302 was strongly additive in the

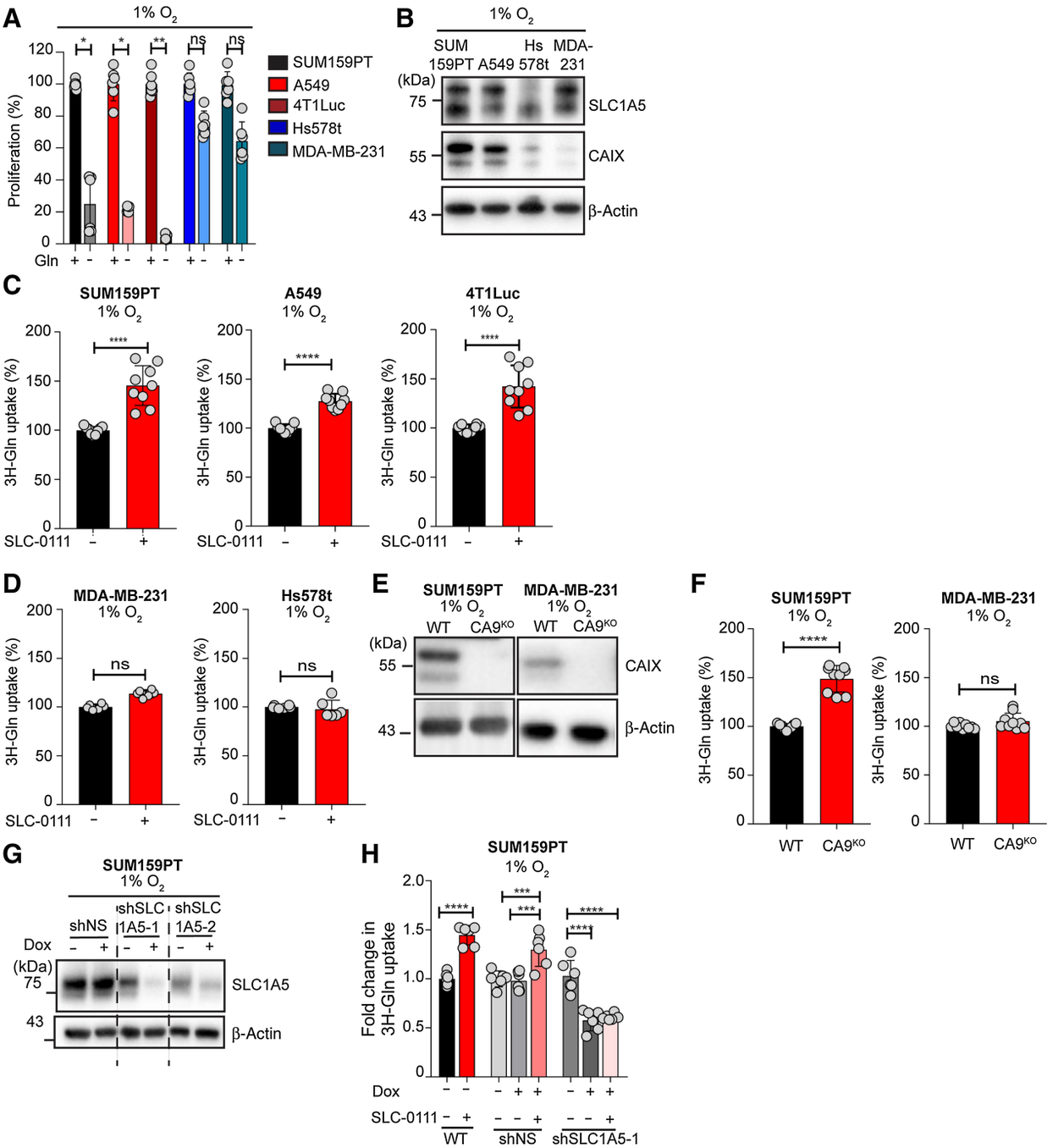

Figure 2.

Loss of CAIX activity increases Gln uptake in hypoxic cancer cells. **A,** Proliferation of the indicated cells in the presence (+) or absence (−) of 4 mmol/L Gln-containing media. **B,** Expression of SLC1A5 and CAIX shown by Western blotting in cell lysates from the indicated cell lines. **C** and **D,** Gln uptake in the indicated cell lines in the presence (+) or absence (−) of 100 μmol/L SLC-0111. **E,** Cellular expression of CAIX shown by Western blotting in cell lysates from WT and *CA9*^{KO} of MDA-MB-231 and SUM159PT cell lines. **F,** Gln uptake in the WT and *CA9*^{KO} of MDA-MB-231 and SUM159PT cell lines. **G,** Cellular expression of SLC1A5 shown by Western blotting in cell lysates from SUM159PT cells expressing shNS and shSLC1A5, cultured in the presence (+) or absence (−) of 0.5 μg/mL Dox. All samples are derived from the same blot and dashed lines indicate juxtaposition of samples from noncontiguous lanes. **H,** Gln uptake in the shNS and shSLC1A5–1 SUM159PT cell lines with the indicated treatments; Dox, 0.5 μg/mL and SLC-0111, 100 μmol/L. All treatments were carried out at 1% O_2 for 72 hours prior to the assay. For all graphs, bars represent means ± SD. For (**A**) statistical significance was assessed using Kruskal–Wallis test on the data from two independent experiments with $n = 3$ (technical replicates) for each experiment. Gln uptake data were assessed by performing Mann–Whitney for (**C**), (**D**), and (**F**), and one-way ANOVA test for (**H**) on data from at least two independent experiments with $n = 3$ for each experiment. *, $P < 0.05$; **, $P < 0.01$; ***, $P < 0.001$; ****, $P < 0.0001$; ns, nonsignificant. See also Supplementary Fig. S2.

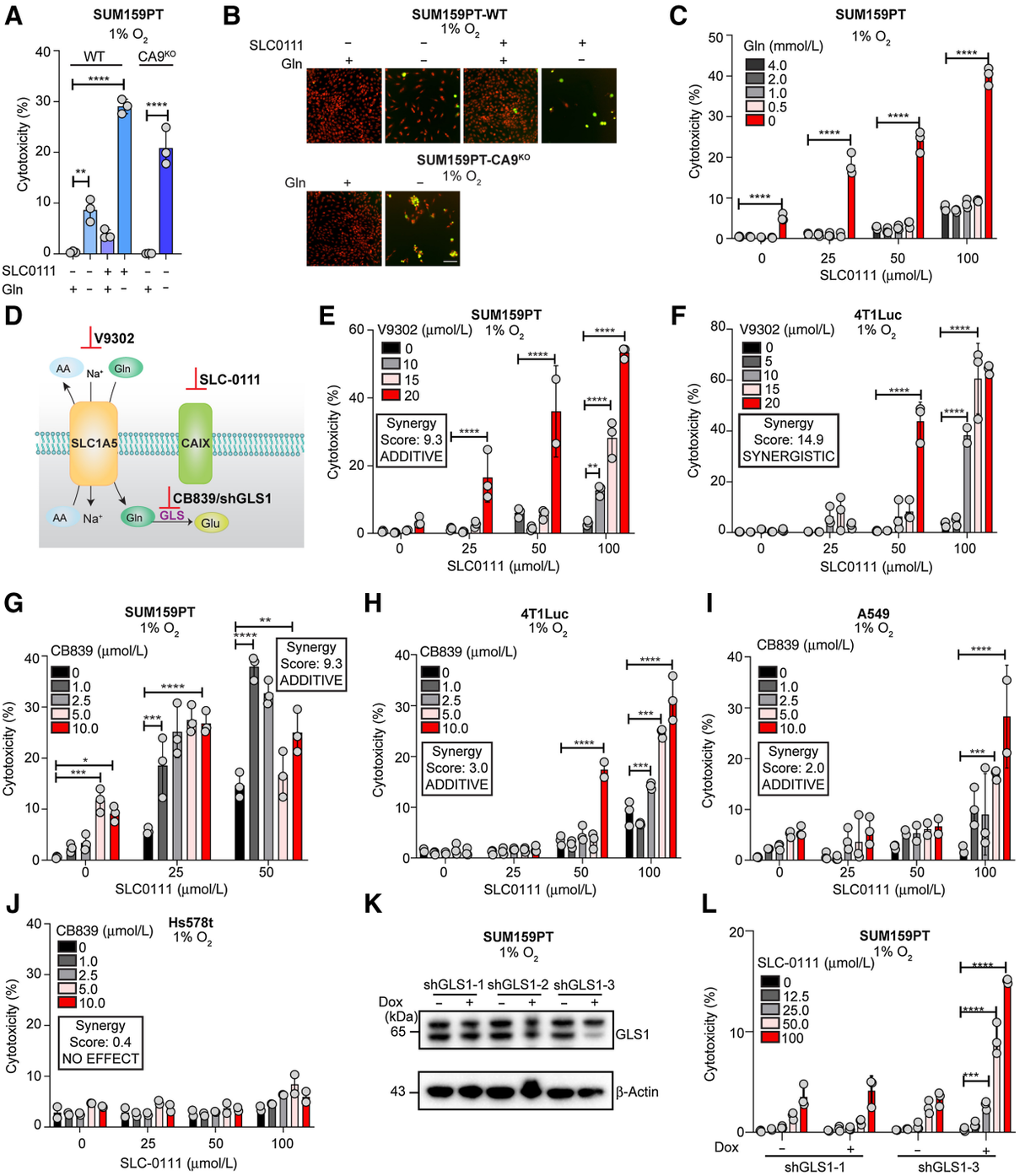

Figure 3.

The combined loss of CAIX/XII activity and Gln metabolism increases cytotoxicity of hypoxic cancer cells. **A,** Cytotoxicity analyses of SUM159PT WT and *CA9*^{KO} cells cultured in the presence (+) or absence (−) of the indicated treatments; SLC-0111, 100 μmol/L, and Gln, 4 mmol/L. **B,** Representative incucyte images for (**A**). Green, cytotoxicity; red, nuclei. **C,** Cytotoxicity analyses of SUM159PT WT cells cultured with indicated concentrations of Gln and SLC-0111. **D,** Graphical representation of the cotargeting strategy and inhibitors used. **E** and **F,** Cell cytotoxicity data for the indicated cell lines cultured with the combination of SLC-0111 and V9302 at the indicated concentrations. **G–J,** Cell cytotoxicity data for the indicated cell lines cultured with the combination of SLC-0111 and CB839 at indicated concentrations. **K,** Cellular expression of GLS1 shown by Western blotting in cell lysates from SUM159PT cells expressing shGLS1, cultured in the presence (+) or absence (−) of 0.5 μg/mL Dox. **L,** Cell cytotoxicity data for SUM159PT sh-GLS1 and 3 cell lines cultured at the indicated SLC-0111 concentrations. All treatments were carried out at 1% O_2 for 72 hours prior to the assay. For all graphs, bars represent means ± SD. Synergy scores and interpretation of the score are provided in boxed insets for each graph. Statistical significance was assessed using two-way ANOVA. Data shown are representative of three independent experiments. *, $P < 0.05$; **, $P < 0.01$; ***, $P < 0.001$; ****, $P < 0.0001$. See also Supplementary Figs. S3 and S4.

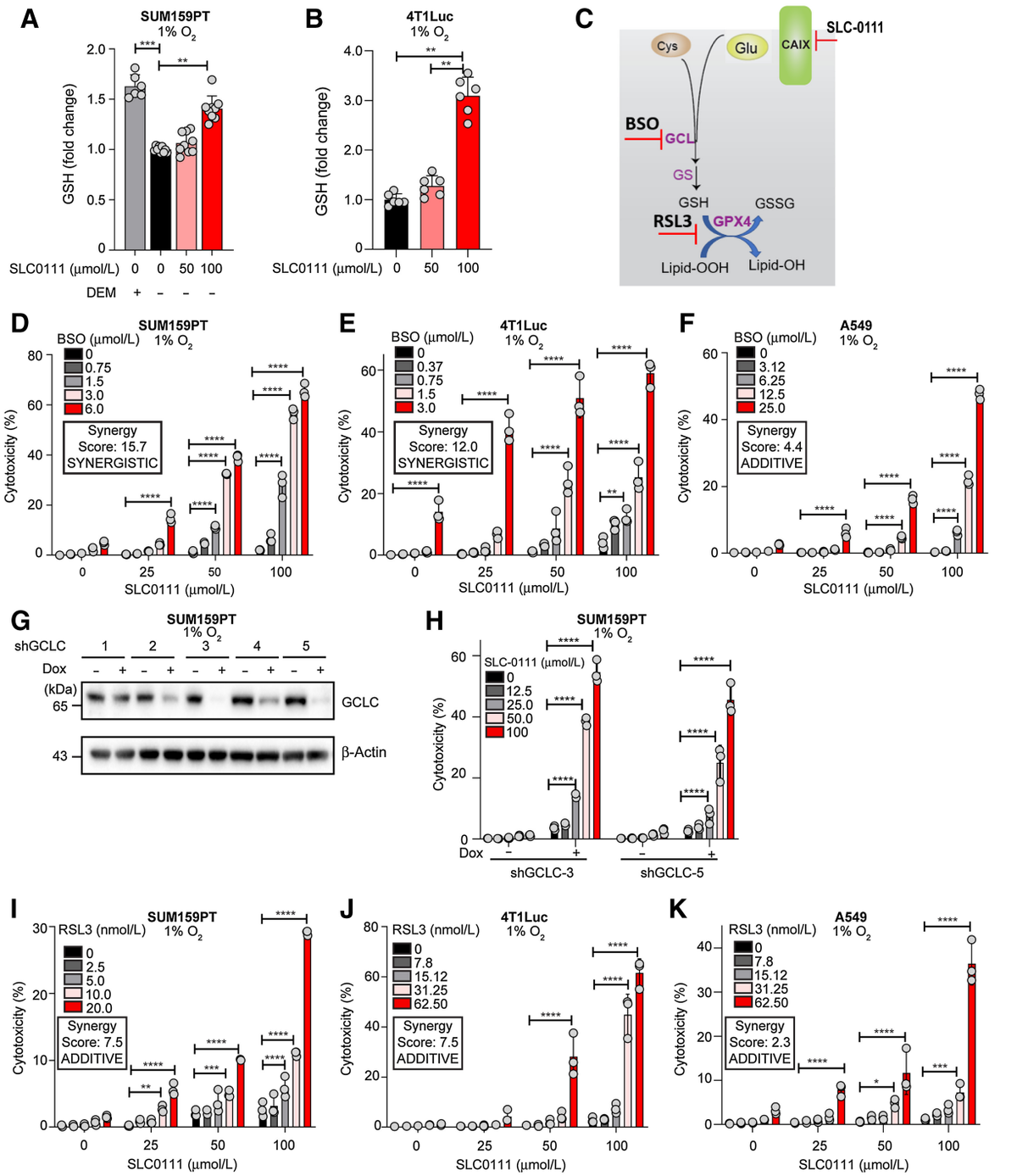

Figure 4.

Loss of CAIX/XII activity increases cellular GSH and prevent cytotoxicity through a GSH/GPX4 axis. **A** and **B,** GSH level in (**A**) SUM159PT-WT and (**B**) 4T1Luc with the treatment of SLC-0111 at indicated concentrations. 0.1 mmol/L diethyl maleate (DEM) was used as a positive control for the assay. **C,** Graphical representation of the cotargeting strategy and inhibitors used. **D–F,** Cell cytotoxicity data of the indicated cell lines with the combination of SLC-0111 and BSO at indicated concentrations. Synergy scores and interpretation of the score are provided in boxed insets for each graph. **G,** Cellular expression of GLS1 shown by Western blotting in cell lysates from SUM159PT cells expressing shGLS1, cultured in the presence (+) or absence (−) of 0.5 μg/mL Dox. **H,** Cell cytotoxicity data of SUM159 sh-GCLC-3 and 5 cell lines at the indicated SLC-0111 concentrations. **I–K,** Cell cytotoxicity data of the indicated cell lines with the combination of SLC-0111 and RSL3 at indicated concentrations. Synergy scores and interpretation of the score are provided in boxed insets for each graph. All treatments were carried out at 1% O_2 for 72 hours prior to the assay. For all graphs, bars indicate means ± SD. Statistical significance was assessed for (**A** and **B**) using one-way ANOVA; Kruskal–Wallis on the data from three independent experiments with $n = 3$. All the cytotoxicity plots were assessed using two-way ANOVA. Data shown are representative of three independent experiments. *, $P < 0.05$; **, $P < 0.01$; ***, $P < 0.001$; ****, $P < 0.0001$. See also Supplementary Fig. S5.

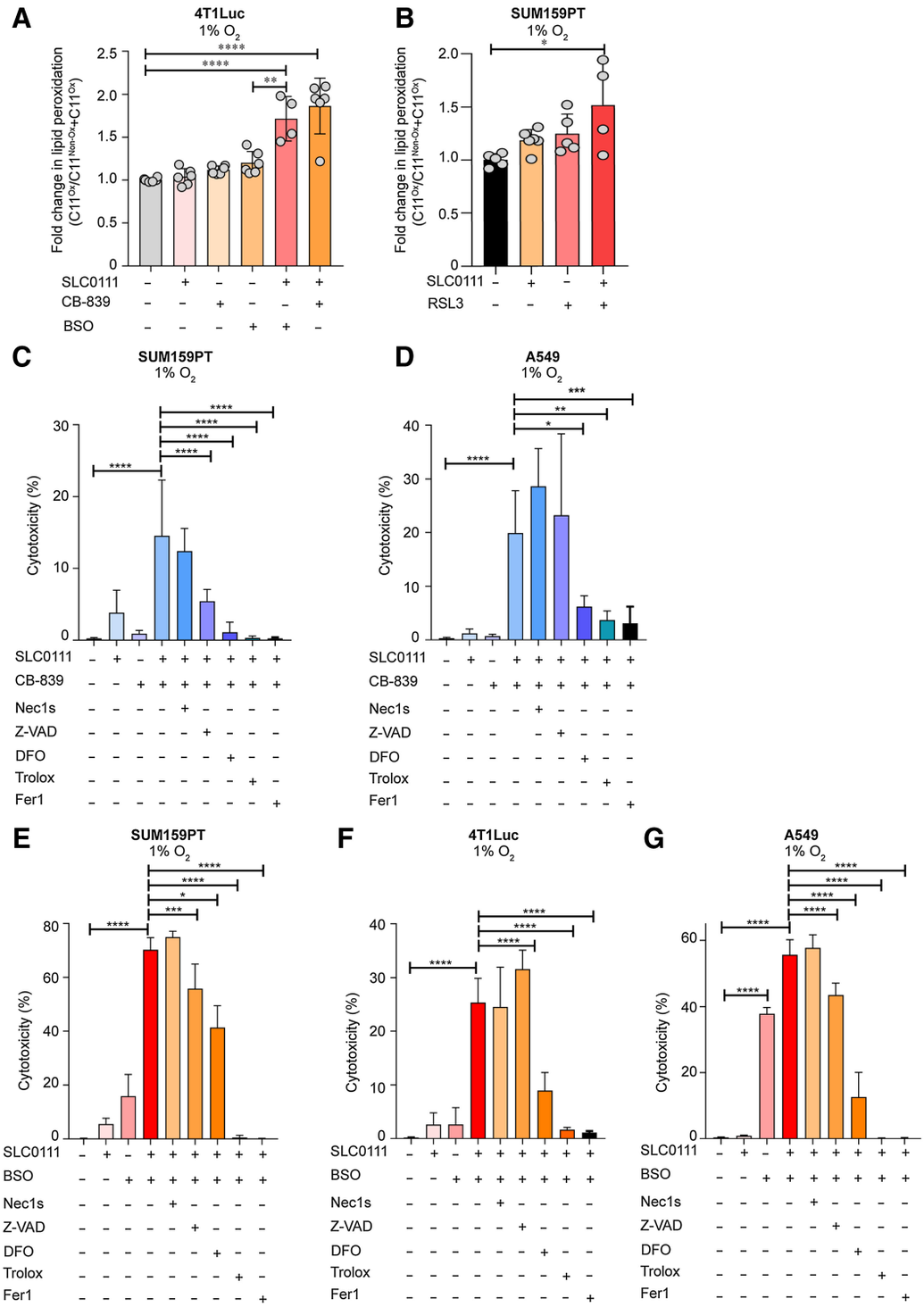

Figure 5.

Combined inhibition of CAIX/XII and Gln metabolism increases lipid peroxidation and induce ferroptosis. **A** and **B,** Lipid peroxidation in (**A**) 4T1Luc and (**B**) SUM159PT cells using BODIPY C11 staining with the indicated treatments; SLC-0111, 100 μmol/L, CB839, 5 μmol/L, BSO, 1.5 μmol/L, RSL3, 10 nmol/L. **C–G,** Cell viability of the indicated cell lines with the combination of CB839 and SLC-0111 (**C** and **D**) or the combination of BSO and SLC-0111 (**E–G**), in the presence of Fer1 (2 μmol/L), Nec1s (50 μmol/L) Z-VAD-fmk (25 μmol/L), DFO (10 μmol/L), Trolox (100 μmol/L). Bars indicate means ± SD. For the lipid peroxidation experiment, statistical significance was assessed using one-way ANOVA on the data from two experiments with $n = 3$. For the cytotoxicity experiments, statistical significance was assessed using two-way ANOVA. Data shown are representative of three independent experiments. All treatments were carried out in hypoxia for 72 hours. *, $P < 0.05$; **, $P < 0.01$; ***, $P < 0.001$; ****, $P < 0.0001$.

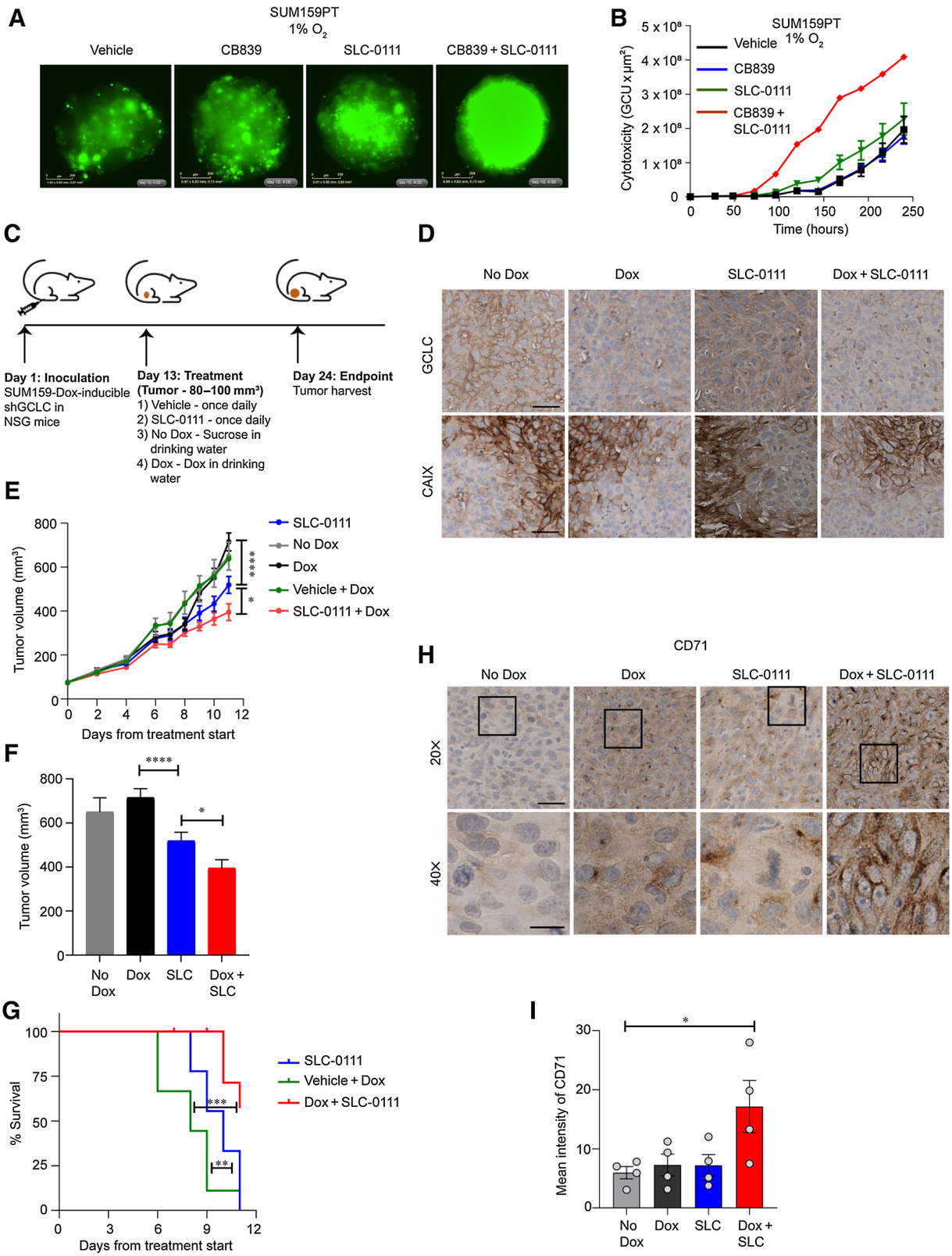
A
SUM159PT
1% O2
Vehicle
CB839
SLC-0111
CB839 + SLC-0111
B
SUM159PT
1% O2
Vehicle
CB839
SLC-0111
CB839 + SLC-0111
Cytotoxicity (GCU x µm²)
Time (hours)
C
Day 1: Inoculation
SUM159-Dox-inducible shGCLC in NSG mice
Day 13: Treatment (Tumor - 80–100 mm³)
1) Vehicle - once daily
2) SLC-0111 - once daily
3) No Dox - Sucrose in drinking water
4) Dox - Dox in drinking water
Day 24: Endpoint
Tumor harvest
D
No Dox
Dox
SLC-0111
Dox + SLC-0111
GCLC
CAIX
E
SLC-0111
No Dox
Dox
Vehicle + Dox
SLC-0111 + Dox
Tumor volume (mm³)
Days from treatment start
F
Tumor volume (mm³)
No Dox
Dox
SLC
Dox + SLC
G
SLC-0111
Vehicle + Dox
Dox + SLC-0111
% Survival
Days from treatment start
H
CD71
No Dox
Dox
SLC-0111
Dox + SLC-0111
20X
40X
I
Mean intensity of CD71
No Dox
Dox
SLC
Dox + SLC

SUM159PT-WT cells (**Fig. 3E**; Supplementary Fig. S3A) and synergistic in the 4T1Luc cells (**Fig. 3F**; Supplementary Fig. S3B).

Next, we combined SLC-0111 treatment with CB839, an inhibitor of the GLS1 enzyme that is important in mediating the first step of Gln catabolism (**Fig. 3D**). The SUM159PT-WT cells showed a dose-dependent increase in cytotoxicity with the combination treatment (SLC-0111 + CB839; **Fig. 3G**). Combination treatments of 4T1Luc and A549 cells also resulted in dose-dependent increases in cytotoxicity relative to single treatments (**Fig. 3H** and **I**). Correspondingly, the combination of the CAIX inhibitor, Compound 11, with CB839 also showed a dose-dependent increase in cytotoxicity of SUM159PT-WT cells (Supplementary Fig. S4A). Analysis of these data using SynergyFinder demonstrated that the combination was additive for all cell lines tested (**Fig. 3G–I**; Supplementary Fig. S3C–S3F). In contrast, the Gln-independent cell line, Hs578t, did not exhibit any increase in cytotoxicity or synergy with the combination treatment (SLC-0111 + CB839; **Fig. 3J**; Supplementary Fig. S3G).

To mitigate off-target effects, we also used Dox-inducible knockdown to specifically target GLS1 expression and tested the combination of GLS1 KD (**Fig. 3K**) with SLC-0111 treatment in the SUM159PT cell line. We observed a dose-dependent cytotoxic response with the SLC-0111 treatment in the cell line in which shRNA results in significant knock down of GLS expression (shGLS1–3), but not when shRNA-mediated knock down is inadequate (shGLS1–1; **Fig. 3L**). Cumulatively, these data suggest that hypoxic cancer cells are vulnerable to perturbations in Gln metabolism following CAIX inhibition.

Loss of CAIX increases GSH levels to prevent cytotoxicity of hypoxic cancer cells through the GSH/GPX4 axis

Having shown that the Gln metabolism plays an important role in hypoxic cancer cells due to inhibition of CAIX function, we sought to investigate the possible route by which Gln is used by hypoxic cancer cells. We recently established the role of CAIX in redox homeostasis maintenance in hypoxic cancer cells, where we showed that inhibition of CAIX leads to increased cellular ROS levels (Supplementary Fig. S4B; ref. 33). This led us to question whether the Gln taken up by the cells upon CAIX inhibition may be used to synthesize the antioxidant, GSH, to overcome oxidative stress and establish redox homeostasis.

To test our hypothesis, we measured the cellular GSH levels following SLC-0111 treatment. In line with our hypothesis, we observed a dose-dependent increase in GSH in SUM159PT-WT and 4T1Luc cell lines (**Fig. 4A** and **B**). We also observed an increase in the GSH to glutathione disulfide (GSSG) ratio following SLC-0111 treatment in the SUM159PT cells (Supplementary Fig. S4C), further suggesting that inhibition of CAIX results in an increased GSH pool. We then measured the cytotoxicity response following combination of SLC-0111 and buthionine sulfoximine (BSO), the inhibitor of glutamate-cysteine ligase catalytic subunit (GCLC) that mediates GSH biosynthesis (**Fig. 4C**). The combination treatment resulted in a dose-dependent increase of cytotoxicity in SUM159PT, 4T1Luc, and A549 cell lines grown in hypoxia (**Fig. 4D–F**). Furthermore, the effect of the combination was synergistic in both breast cancer cell lines (**Fig. 4D** and **E**; Supplementary Fig. S5A and S5B) and was additive in the A549 cells (**Fig. 4F**; Supplementary Fig. S5C).

We confirmed this finding using the combination of SLC-0111 treatment with the knockdown of GCLC in SUM159PT (shGCLC) cells. First, we screened several Dox-inducible shRNA constructs targeting GCLC (shGCLC) for levels of knockdown in the presence of Dox (**Fig. 4G**), and used the two cell lines showing the highest levels of depletion of GCLC for subsequent evaluation of levels of cytotoxicity. We observed a dose-dependent increase in cytotoxicity following SLC-0111 treatment in the cell lines effectively depleting GCLC levels (shGCLC-3 and shGCLC-5), without any cytotoxic effects in the corresponding no-Dox treatment controls (**Fig. 4H**).

Next, we sought to identify whether the GSH activity is important for mediating the function of GPX4 enzyme and prevent lipid peroxidation. We tested the combination of SLC-0111 with the GPX4 inhibitor, RSL3, and observed a dose-dependent, additive increase of cytotoxicity with the combination in SUM159PT, 4T1Luc and A549 cell lines (**Fig. 4I–K**; Supplementary Fig. S5D–S5F). These data suggest that the increased uptake in Gln following CAIX inhibition is to maintain GSH stores to sustain the GSH/GPX4 axis to maintain cell survival, thus identifying a combination strategy to enhance cell cytotoxicity of hypoxic tumor cells.

The combined inhibition of CAIX activity and Gln metabolism increases lipid peroxidation and induces ferroptosis

Our data indicate the involvement of the GSH/GPX4 axis upon CAIX inhibition in hypoxic cancer cells, possibly for preventing lipid peroxidation. To test this, we evaluated lipid peroxidation in hypoxic cancer cells with single treatments or combination treatments described earlier. We observed a significant increase in lipid peroxidation following combination of SLC-0111 with CB839, BSO, or RSL3, compared with the corresponding single treatments (**Fig. 5A** and **B**). Such an increase in lipid peroxidation and increased cytotoxicity in the absence of the antioxidant system (**Fig. 4D–K**) are hallmarks of ferroptosis.

This led us to assess whether the cytotoxicity observed by combining the inhibition of CAIX and Gln metabolism is mediated by ferroptosis. To investigate this possibility, we induced cytotoxicity in hypoxic cancer cells by combining CB839 and SLC-0111 treatment as before and assessed whether this cytotoxicity is rescued by blocking apoptosis, necroptosis or ferroptosis. As observed earlier, the cytotoxicity increases with the combination compared with the single treatments. The addition of necroptosis inhibitor, necrostatin-1 (Nec1s), had no effect on cell death in both SUM159PT and A549 cell lines (**Fig. 5C** and **D**). Addition of the apoptosis inhibitor, ZVAD-fmk had no effect of

Figure 6.

Cotargeting CAIX/XII activity and GSH synthesis decreases the tumor growth. **A,** Cytotoxicity (green) in tumor spheroids treated with CB839 (1 μmol/L), SLC0111 (100 μmol/L) or the combination (CB839+SLC-0111). Tumor spheroids were cultured at 21% O_2 for 10 days and monitored real time. **B,** Quantification of cytotoxicity in tumor speroids from (**A**). **C,** Schematic of the *in vivo* study design and treatment. **D,** IHC staining showing the expression of GCLC and CAIX in representative tumor sections from the indicated treatment groups. Scale bar, 50 μm. **E,** Tumor growth curve of SUM159PT sh-GCLC tumors with indicated treatments, $n = 8$ to 9 per group. **F,** Tumor growth at endpoint of SUM159PT sh-GCLC tumors with indicated treatments, $n = 8$ to 9 per group. **G,** Survival plot for SUM159-shGCLC tumors in the indicated treatment groups. **H,** IHC staining showing the expression of CD71 (Transferrin receptor) in representative tumor sections from the indicated treatment groups. Scale bar 50 μm for 20× magnification and 25 μm for 40× magnification images. **I,** Quantification of the mean intensity of CD71 signal from IHC images of tumor sections in the indicated treatment groups. Quantification was performed on at least 4 images per tumor section with $n = 4$ mice per group. Bars in panels **B**, **E**, and **F** indicate means ± SEM. Bars in panel I indicate means ± SD. The statistical significance for tumor growth curve was assessed using two-way ANOVA. Tumor growth at endpoint and the mean intensity for CD71 were assessed using one-way ANOVA. *, $P < 0.05$; ****, $P < 0.0001$. See also Supplementary Fig. S6.

rescuing cell death in the A549 cell line, but moderately rescued the SUM159PT cell line from cell death. However, the rescue observed with ZVAD-fmk in SUM159PT is less than 50%. In contrast, the addition of ferroptosis inhibitor, Ferrostatin-1 (Fer-1) or an antioxidant such as Trolox (Tro) completely rescued this cytotoxicity (**Fig. 5C** and **D**). In addition, the iron chelator, deferoxamine (DFO), also rescued the cells from cytotoxic effects (**Fig. 5C** and **D**).

A similar trend is observed with the inhibition of GSH synthesis and CAIX activity, where the cytotoxicity elicited with the combination of treatment with BSO and SLC-0111 in the SUM159PT, 4T1Luc and A549 cells is prevented in the presence of Fer-1, Tro, or DFO, with a moderate rescue in the presence of ZVAD-fmk and no effects with Nec1s (**Fig. 5E–G**). These data suggest that the combined inhibition of CAIX activity and Gln metabolism increases lipid peroxidation and induces the iron-dependent oxidative cell death, ferroptosis.

Cotargeting CAIX/XII activity and GSH synthesis decreases the tumor growth and improves survival

Next, we evaluated the effect of the combination of SLC-0111 and CB839 on the level of cytotoxicity by SUM159PT cancer cells grown as spheroids to better model the potential impact of combination treatment on cell viability in 3 dimensional (3D) cultures. Similar to our findings in monolayer cultures, we observed a significant increase in the level of cytotoxicity with the drug combination compared with the single treatments (**Fig. 6A** and **B**).

To study the effects of cotargeting CAIX and GSH synthesis *in vivo*, we used the SUM159PT cells expressing Dox-inducible shGCLC-5 (see **Fig. 4G**), enabling us to couple Dox-inducible genetic knockdown of GCLC expression with pharmacologic inhibition of CAIX activity. The SUM159PT Dox-inducible shGCLC cells were injected into the mammary fat pad of NSG mice and administration of Dox and/or SLC-0111 was initiated after the tumors were established (**Fig. 6C**). IHC analyses of tumor tissue sections confirmed both effective depletion of GCLC in response to Dox administration and strong, regional expression of CAIX across all treatment groups (**Fig. 6D**). Dox-inducible depletion of GCLC expression alone had no impact on tumor volume, compared with control tumors, suggesting that targeting GCLC on its own does not suppress tumor growth (**Fig. 6E** and **F**). In contrast, treatment with SLC-0111 as a single agent reduced the tumor volume compared with the control group (**Fig. 6E** and **F**), and combined targeting of GCLC and CAIX resulted in a further significant reduction in tumor growth (**Fig. 6E** and **F**). Furthermore, cotargeting GCLC and CAIX significantly increased survival of the mice, compared with targeting these proteins individually (**Fig. 6G**).

We then assessed whether the cotargeting of CAIX and GCLC increases lipid peroxidation and induces ferroptosis in the tumors as observed in the *in vitro* studies. To test this, we performed IHC on tumor tissue sections from the treatment groups to determine the levels of expression of 4-HNE, an established marker of lipid peroxidation and oxidative stress (43), and CD71 (also known as transferrin receptor 1; TfR1), which recently was identified as a marker of ferroptosis in tumors (44). We observed that inhibition of CAIX and GCLC increased levels of 4-HNE, compared with control tumors (Supplementary Fig. S6). Moreover, the expression of CD71 was significantly increased in the tumors from animals in which GCLC and CAIX were targeted in combination, compared with either of the single treatment groups (**Fig. 6H** and **I**). These data provide proof of concept that cotargeting of CAIX and GSH synthesis could be an effective strategy to treat hypoxic solid tumors.

Discussion

Metabolic plasticity in solid tumors promotes adaptation and resistance to single therapy strategies by initiating compensatory mechanisms (45, 46). A major metabolic shift in hypoxic cancer cells is the metabolic reprogramming to support glycolysis. Although this shift is important for ATP production, it also attenuates ROS generation by preventing the flux of carbons into the tricarboxylic acid (TCA) cycle and oxidative phosphorylation (6). ROS acts as a double-edged sword in cancer cells. While a relatively higher ROS level compared with normal cells promotes tumorigenesis and metastasis, excessive ROS could have deleterious effects and cause cell death (47). Hence, cancer cells maintain redox equilibrium by deploying antioxidant systems. In this study, we demonstrate a potential mechanism by which Gln-dependent, hypoxic cancer cells adapt to oxidative stress associated with inhibition of CAIX, a therapeutic target in hypoxic tumors (19, 20, 28, 29, 31, 48). We have found that CAIX associates with the Gln transporter, SLC1A5 in hypoxic cancer cells. We find that this association is independent of the catalytic activity of CAIX, but is dependent on the intracellular domain of CAIX. It is not clear at present as to whether this association is direct or is mediated by other proteins. Functionally, however, we find that CAIX activity can regulate Gln uptake through SLC1A5. Interestingly, the pharmacologic inhibition of CAIX activity, or genetic knockdown of CAIX expression, results in an increase in Gln uptake only in Gln-dependent cancer cells, suggesting that under hypoxic conditions resulting in the expression of CAIX, such cells compensate for the survival stress by increased uptake of extracellular Gln. Indeed, CAIX inhibition in tumor cells grown under Gln-deprived conditions undergo significant cell death.

The increased levels of expression of SLC1A5 in response to CAIX KO may be a compensatory response by the cells to increased oxidative stress in hypoxia resulting from CAIX inhibition. The precise mechanism by which reduced CAIX expression leads to increased SLC1A5 expression remains a focus of future studies.

Furthermore, our data demonstrate that while the intracellular domain of CAIX mediates the association of CAIX with SLC1A5, the regulation of SLC1A5-mediated Gln uptake by CAIX appears to require both the extracellular catalytic domain as well as the intracellular domain. Although these observations do not clarify the precise mechanism of action of CAIX regulation of Gln uptake by SLC1A5, it is likely that the mechanism requires CAIX activity, because the intracellular domain of CAIX has been demonstrated to regulate the extracellular catalytic activity of CAIX via an "inside-out" signaling mechanism requiring protein kinase A (PKA) mediated phosphorylation of the intracellular domain (49). Thus, deletion of the intracellular domain would inhibit CAIX activity and result in increased Gln uptake by SLC1A5. Overall, our data suggest that the close association of CAIX and SLC1A5 functionally regulate SLC1A5 function and that this regulation requires CAIX enzymatic activity.

Our data further suggest that some of this Gln may be used for GSH synthesis to maintain redox balance through the GSH/GPX4 axis to prevent ferroptosis. Critically, this metabolic dependency makes the tumor cells more vulnerable to ferroptosis when both CAIX and critical nodes of the Gln metabolism pathway leading to GSH synthesis are inhibited simultaneously. Thus, our novel findings reveal an important connection between CAIX and Gln metabolism in the hypoxic microenvironment. Stable isotope tracing studies in the context of inhibition of CAIX to determine the relative contribution

of Gln-derived glutamate to GSH synthesis versus the TCA cycle are the subject of future investigations.

Tumor hypoxia presents a major barrier for the treatment of cancer and one of the mechanisms by which hypoxic cancer cells achieve this is by resisting apoptosis by selectively expanding the cell population with p53 mutations (50). Therefore, targeting other modes of regulated cell death could be more effective for the treatment of hypoxic tumors. Recently, our group identified genes involved in redox homeostasis that play an important role in antioxidant defense to be synthetic lethal with CAIX (33). Furthermore, we demonstrated that functional inhibition of CAIX causes an increase in cellular ROS (33). In the current study, we provide further insight into the compensatory mechanism that hypoxic cancer cells deploy to prevent oxidative stress associated with CAIX inhibition and promote survival. When CAIX inhibition is combined with the loss of GSH/GPX4 antioxidant axis, it leads to lipid peroxidation and eventually ferroptosis. Extensive research on ferroptosis in the past decade has led to the identification of ferroptosis inducers (FIN). While many of the FINs have proven to be effective in targeting cancer cells *in vitro* and *in vivo*, none have progressed to clinical evaluation (51, 52). Hence, identifying ferroptosis regulating targets that already have well-established small molecule inhibitors will accelerate the clinical translation process. Our study has evaluated the effect of combining SLC-0111 with inhibitors targeting various nodes of Gln metabolism and our data show that the combinations significantly enhance ferroptosis, but not apoptosis or necroptosis. Given that SLC-0111 is a clinical stage inhibitor (29) with specificity to target hypoxic cancers, our findings will be beneficial in developing novel treatment strategies. In particular, the combination of SLC-0111 with the GLS1 inhibitor, CB839, is of potential clinical relevance as CB839 is well advanced in clinical trials and has shown promising effects (NCT03450018). Furthermore, our data provides evidence that SLC-0111 treatment significantly potentiates the therapeutic effect of CB839 *in vitro*.

In summary, to our knowledge, this is the first study to show evidence suggesting a connection between CAIX and Gln metabolism. In addition, our study reveals a novel adaptation mechanism by hypoxic cancer cells to prevent oxidative stress associated with the inhibition of CAIX. Furthermore, we identify cotargeting strategies to overcome this adaptation by combining inhibitors of the Gln/GSH metabolic axis with CAIX inhibition. Our findings open a new area of investigation in understating the molecular details of the CAIX–SLC1A5 interaction, and novel combinatorial therapeutic strategies for hypoxic tumors.

Limitations of the study

While we have validated the interaction of CAIX and SLC1A5 identified previously through BioID (22), it remains unclear whether the interaction is direct or indirect, involving yet to be identified intermediary proteins. In addition, it is not entirely clear from our study as to whether the interaction is critical for the observed effects on Gln uptake upon inhibition of CAIX activity and expression. Our findings, through targeting specific metabolic nodes in the Gln to GSH pathway, suggest that the increased Gln uptake in Gln-dependent, CAIX-inhibited cells may contribute to the observed GSH levels under these conditions. However, detailed metabolic tracing experiments will be required in the future to identify the precise path(s) taken by the increased Gln.

Authors' Disclosures

P.C. McDonald reports grants from Canadian Institutes of Health Research; and grants from Canadian Cancer Society during the conduct of the study; other support from SignalChem Lifesciences Corporation outside the submitted work; in addition, P.C. McDonald has a patent for US 9463171 B2 issued; and SignalChem Lifesciences Corporation - Royalties issued as a result of intellectual property agreement. S. Dedhar reports grants from Canadian Institutes for Health Research during the conduct of the study; other support from Signal Chem Lifesciences Corp outside the submitted work; in addition, S. Dedhar has a patent for US9463171B2 issued; and Royalties issued as result of intellectual property. No disclosures were reported by the other authors.

Authors' Contributions

G. Venkateswaran: Conceptualization, formal analysis, supervision, validation, investigation, methodology, writing–original draft, writing–review and editing. **P.C. McDonald:** Conceptualization, formal analysis, supervision, investigation, methodology, writing–original draft, writing–review and editing. **S.C. Chafe:** Conceptualization, supervision, validation, investigation, methodology, writing–review and editing. **W.S. Brown:** Formal analysis, investigation, methodology. **Z.J. Gerbec:** Formal analysis, investigation, methodology. **S.J. Awrey:** Formal analysis, investigation. **S.J. Parker:** Formal analysis, investigation, methodology, writing–review and editing. **S. Dedhar:** Conceptualization, supervision, funding acquisition, methodology, writing–original draft, writing–review and editing.

Acknowledgments

This research was supported by the Canadian Institutes of Health Research (CIHR) grant FDN-143318 awarded to S. Dedhar. This work was also supported by CIHR grant AWD-020801 awarded to S. Parker.

The publication costs of this article were defrayed in part by the payment of publication fees. Therefore, and solely to indicate this fact, this article is hereby marked "advertisement" in accordance with 18 USC section 1734.

Note

Supplementary data for this article are available at Molecular Cancer Therapeutics Online (http://mct.aacrjournals.org/).

Received January 19, 2023; revised May 18, 2023; accepted June 20, 2023; published first June 22, 2023.

References

1. Wicks EE, Semenza GL. Hypoxia-inducible factors: cancer progression and clinical translation. J Clin Invest 2022;132:e159839.
2. Vaupel P, Thews O, Hoeckel M. Treatment resistance of solid tumors: role of hypoxia and anemia. Med Oncol 2001;18:243–59.
3. Moeller BJ, Cao Y, Li CY, Dewhirst MW. Radiation activates HIF-1 to regulate vascular radiosensitivity in tumors: role of reoxygenation, free radicals, and stress granules. Cancer Cell 2004;5:429–41.
4. Parks SK, Cormerais Y, Pouyssegur J. Hypoxia and cellular metabolism in tumor pathophysiology. J Physiol 2017;595:2439–50.
5. Lee P, Chandel NS, Simon MC. Cellular adaptation to hypoxia through hypoxia inducible factors and beyond. Nat Rev Mol Cell Biol 2020;21:268–83.
6. Kim JW, Tchernyshyov I, Semenza GL, Dang CV. HIF-1-mediated expression of pyruvate dehydrogenase kinase: a metabolic switch required for cellular adaptation to hypoxia. Cell Metab 2006;3:177–85.
7. Parks SK, Chiche J, Pouyssegur J. pH control mechanisms of tumor survival and growth. J Cell Physiol 2011;226:299–308.
8. Becker HM, Deitmer JW. Transport metabolons and acid/base balance in tumor cells. Cancers 2020;12:899.
9. Mboge MY, Mahon BP, McKenna R, Frost SC. Carbonic anhydrases: role in pH control and cancer. Metabolites 2018;8:19.
10. Korkeila E, Talvinen K, Jaakkola PM, Minn H, Syrjanen K, Sundstrom J, et al. Expression of carbonic anhydrase IX suggests poor outcome in rectal cancer. Br J Cancer 2009;100:874–80.

11. Loncaster JA, Harris AL, Davidson SE, Logue JP, Hunter RD, Wycoff CC, et al. Carbonic anhydrase (CA IX) expression, a potential new intrinsic marker of hypoxia: correlations with tumor oxygen measurements and prognosis in locally advanced carcinoma of the cervix. Cancer Res 2001;61:6394–9.
12. Chia SK, Wykoff CC, Watson PH, Han C, Leek RD, Pastorek J, et al. Prognostic significance of a novel hypoxia-regulated marker, carbonic anhydrase IX, in invasive breast carcinoma. J Clin Oncol 2001;19:3660–8.
13. Ilie M, Mazure NM, Hofman V, Ammadi RE, Ortholan C, Bonnetaud C, et al. High levels of carbonic anhydrase IX in tumor tissue and plasma are biomarkers of poor prognostic in patients with non–small cell lung cancer. Br J Cancer 2010; 102:1627–35.
14. Klatte T, Seligson DB, Rao JY, Yu H, de Martino M, Kawaoka K, et al. Carbonic anhydrase IX in bladder cancer: a diagnostic, prognostic, and therapeutic molecular marker. Cancer 2009;115:1448–58.
15. McIntyre A, Patiar S, Wigfield S, Li JL, Ledaki I, Turley H, et al. Carbonic anhydrase IX promotes tumor growth and necrosis *in vivo* and inhibition enhances anti-VEGF therapy. Clin Cancer Res 2012;18:3100–11.
16. Tan EY, Yan M, Campo L, Han C, Takano E, Turley H, et al. The key hypoxia regulated gene CAIX is upregulated in Basal-like breast tumors and is associated with resistance to chemotherapy. Br J Cancer 2009;100:405–11.
17. Generali D, Fox SB, Berruti A, Brizzi MP, Campo L, Bonardi S, et al. Role of carbonic anhydrase IX expression in prediction of the efficacy and outcome of primary epirubicin/tamoxifen therapy for breast cancer. Endocr Relat Cancer 2006;13:921–30.
18. Koukourakis MI, Giatromanolaki A, Sivridis E, Simopoulos K, Pastorek J, Wykoff CC, et al. Hypoxia-regulated carbonic anhydrase-9 (CA9) relates to poor vascularization and resistance of squamous cell head and neck cancer to chemoradiotherapy. Clin Cancer Res 2001;7:3399–403.
19. Lock FE, McDonald PC, Lou Y, Serrano I, Chafe SC, Ostlund C, et al. Targeting carbonic anhydrase IX depletes breast cancer stem cells within the hypoxic niche. Oncogene 2013;32:5210–9.
20. Lou Y, McDonald PC, Oloumi A, Chia S, Ostlund C, Ahmadi A, et al. Targeting tumor hypoxia: suppression of breast tumor growth and metastasis by novel carbonic anhydrase IX inhibitors. Cancer Res 2011;71:3364–76.
21. Chiche J, Ilc K, Laferriere J, Trottier E, Dayan F, Mazure NM, et al. Hypoxia-inducible carbonic anhydrase IX and XII promote tumor cell growth by counteracting acidosis through the regulation of the intracellular pH. Cancer Res 2009;69:358–68.
22. Swayampakula M, McDonald PC, Vallejo M, Coyaud E, Chafe SC, Westerback A, et al. The interactome of metabolic enzyme carbonic anhydrase IX reveals novel roles in tumor cell migration and invadopodia/MMP14-mediated invasion. Oncogene 2017;36:6244–61.
23. Chafe SC, Lou Y, Sceneay J, Vallejo M, Hamilton MJ, McDonald PC, et al. Carbonic anhydrase IX promotes myeloid-derived suppressor cell mobilization and establishment of a metastatic niche by stimulating G-CSF production. Cancer Res 2015;75:996–1008.
24. Svastova E, Witarski W, Csaderova L, Kosik I, Skvarkova L, Hulikova A, et al. Carbonic anhydrase IX interacts with bicarbonate transporters in lamellipodia and increases cell migration via its catalytic domain. J Biol Chem 2012;287:3392–402.
25. Hsieh MJ, Chen KS, Chiou HL, Hsieh YS. Carbonic anhydrase XII promotes invasion and migration ability of MDA-MB-231 breast cancer cells through the p38 MAPK signaling pathway. Eur J Cell Biol 2010;89:598–606.
26. Pastorekova S, Gillies RJ. The role of carbonic anhydrase IX in cancer development: links to hypoxia, acidosis, and beyond. Cancer Metastasis Rev 2019;38:65–77.
27. Pacchiano F, Carta F, McDonald PC, Lou Y, Vullo D, Scozzafava A, et al. Ureido-substituted benzenesulfonamides potently inhibit carbonic anhydrase IX and show antimetastatic activity in a model of breast cancer metastasis. J Med Chem 2011;54:1896–902.
28. McDonald PC, Chafe SC, Brown WS, Saberi S, Swayampakula M, Venkateswaran G, et al. Regulation of pH by carbonic anhydrase 9 mediates survival of pancreatic cancer cells with activated KRAS in response to hypoxia. Gastroenterology 2019;157:823–37.
29. McDonald PC, Chia S, Bedard PL, Chu Q, Lyle M, Tang L, et al. A phase 1 study of SLC-0111, a novel inhibitor of carbonic anhydrase IX, in patients with advanced solid tumors. Am J Clin Oncol 2020;43:484–90.
30. Boyd NH, Walker K, Fried J, Hackney JR, McDonald PC, Benavides GA, et al. Addition of carbonic anhydrase 9 inhibitor SLC-0111 to temozolomide treatment delays glioblastoma growth *in vivo*. JCI Insight 2017;2:e92928.
31. Chafe SC, McDonald PC, Saberi S, Nemirovsky O, Venkateswaran G, Burugu S, et al. Targeting hypoxia-induced carbonic anhydrase IX enhances immune-checkpoint blockade locally and systemically. Cancer Immunol Res 2019;7: 1064–78.
32. Lou Y, Preobrazhenska O, auf dem Keller U, Sutcliffe M, Barclay L, McDonald PC, et al. Epithelial–mesenchymal transition (EMT) is not sufficient for spontaneous murine breast cancer metastasis. Dev Dyn 2008;237:2755–68.
33. Chafe SC, Vizeacoumar FS, Venkateswaran G, Nemirovsky O, Awrey S, Brown WS, et al. Genome-wide synthetic lethal screen unveils novel CAIX-NFS1/xCT axis as a targetable vulnerability in hypoxic solid tumors. Sci Adv 2021;7: eabj0364.
34. Ianevski A, Giri AK, Aittokallio T. SynergyFinder 3.0: an interactive analysis and consensus interpretation of multidrug synergies across multiple samples. Nucleic Acids Res 2022;50:W739–w43.
35. Magtanong L, Ko P-J, To M, Cao JY, Forcina GC, Tarangelo A, et al. Exogenous monounsaturated fatty acids promote a ferroptosis-resistant cell state. Cell Chem Biol 2019;26:420–32.
36. Parker SJ, Amendola CR, Hollinshead KER, Yu Q, Yamamoto K, Encarnación-Rosado J, et al. Selective alanine transporter utilization creates a targetable metabolic niche in pancreatic cancer. Cancer Discov 2020;10:1018–37.
37. Zhou S, Xie J, Yu C, Feng Z, Cheng K, Ma J, et al. CD226 deficiency promotes glutaminolysis and alleviates mitochondria damage in vascular endothelial cells under hemorrhagic shock. Faseb j 2021;35:e21998.
38. Cormerais Y, Vucetic M, Pouysségur J. Targeting amino acids transporters (SLCs) to starve cancer cells to death. Biochem Biophys Res Commun 2019;520: 691–93.
39. Liu Y, Zhao T, Li Z, Wang L, Yuan S, Sun L. The role of ASCT2 in cancer: a review. Eur J Pharmacol 2018;837:81–87.
40. Hegazy M, Cohen-Barak E, Koetsier JL, Najor NA, Arvanitis C, Sprecher E, et al. Proximity ligation assay for detecting protein–protein interactions and protein modifications in cells and tissues *in situ*. Curr Protoc Cell Biol 2020;89:e115.
41. Schulte ML, Fu A, Zhao P, Li J, Geng L, Smith ST, et al. Pharmacologic blockade of ASCT2-dependent glutamine transport leads to antitumor efficacy in preclinical models. Nat Med 2018;24:194–202.
42. Broer A, Fairweather S, Broer S. Disruption of amino acid homeostasis by novel ASCT2 inhibitors involves multiple targets. Front Pharmacol 2018;9:785.
43. Zhang HF, Hughes CS, Li W, He JZ, Surdez D, El-Naggar AM, et al. Proteomic screens for suppressors of anoikis identify IL1RAP as a promising surface target in Ewing sarcoma. Cancer Discov 2021;11:2884–903.
44. Feng H, Schorpp K, Jin J, Yozwiak CE, Hoffstrom BG, Decker AM, et al. Transferrin receptor is a specific ferroptosis marker. Cell Rep 2020;30:3411–23.
45. Momcilovic M, Bailey ST, Lee JT, Fishbein MC, Braas D, Go J, et al. The GSK3 signaling axis regulates adaptive glutamine metabolism in lung squamous cell carcinoma. Cancer Cell 2018;33:905–21.
46. Biancur DE, Paulo JA, Malachowska B, Quiles Del Rey M, Sousa CM, Wang X, et al. Compensatory metabolic networks in pancreatic cancers upon perturbation of glutamine metabolism. Nat Commun 2017;8:15965.
47. Reczek CR, Chandel NS. The two faces of reactive oxygen species in cancer. Ann Rev Cancer Biol 2017;1:79–98.
48. Supuran CT. Experimental carbonic anhydrase inhibitors for the treatment of hypoxic tumors. J Exp Pharmacol 2020;12:603–17.
49. Ditte P, Dequiedt F, Svastova E, Hulikova A, Ohradanova-Repic A, Zatovicova M, et al. Phosphorylation of carbonic anhydrase IX controls its ability to mediate extracellular acidification in hypoxic tumors. Cancer Res 2011;71:7558–67.
50. Graeber TG, Osmanian C, Jacks T, Housman DE, Koch CJ, Lowe SW, et al. Hypoxia-mediated selection of cells with diminished apoptotic potential in solid tumors. Nature 1996;379:88–91.
51. Hadian K, Stockwell BR. A roadmap to creating ferroptosis-based medicines. Nat Chem Biol 2021;17:1113–16.
52. Wang H, Lin D, Yu Q, Li Z, Lenahan C, Dong Y, et al. A promising future of ferroptosis in tumor therapy. Front Cell Devel Biol 2021;9:629150.